Self-Guiding Polymeric Prodrug Micelles with Two Aggregation-Induced Emission Photosensitizers for Enhanced Chemo-Photodynamic Therapy

Xiaoqing Yi, [†,a,b] Jing-Jing Hu, [†,a] Jun Dai,[c] Xiaoding Lou,[,a] Zujin Zhao,[e] Fan Xia, [*,a] and Ben Zhong Tang[*,d,e]*

[a] Engineering Research Center of Nano-Geomaterials of Ministry of Education, Faculty of Materials Science and Chemistry, China University of Geosciences, Wuhan 430074, China.

[b] Key Laboratory of Prevention and Treatment of Cardiovascular and Cerebrovascular Diseases, Ministry of Education, Key Laboratory of Biomaterials and Biofabrication in Tissue Engineering of Jiangxi Province, Gannan Medical University, Ganzhou 341000, China.

[c] Department of Obstetrics and Gynecology, Tongji Hospital, Tongji Medical College, Huazhong University of Science and Technology, Wuhan 430074, China.

[d] Department of Chemistry, Hong Kong Branch of Chinese National Engineering Research Center for Tissue Restoration and Reconstruction, The Hong Kong University of Science and Technology, Clear Water Bay, Kowloon, Hong Kong, China

[e] State Key Laboratory of Luminescent Materials and Devices, Guangdong Provincial Key Laboratory of Luminescence from Molecular Aggregates, South China University of Technology, Guangzhou 510640, China.

* Corresponding author. E-mail: louxiaoding@cug.edu.cn (X. Lou).

xiafan@cug.edu.cn (F. Xia).

tangbenz@ust.hk (B. Z. Tang).

† These authors contributed equally to this work.

ABSTRACT: Nowadays, aggregation-induced emission luminogens (AIEgens) with reactive oxygen species (ROS) generating ability have been used as photosensitizers for imaging guided photodynamic therapy (PDT). To achieve enhanced antitumor outcomes, combining AIEgens-based PDT with chemotherapy is an efficient strategy. However, the therapeutic efficiency is hampered by the limited cellular uptake efficiency and the appropriate light irradiation occasion. In this paper, a self-guiding polymeric micelle (TB@PMPT) composed of two AIE photosensitizers and a reduction-sensitive paclitaxel prodrug (PTX-SS-N_3) was established for enhanced chemo-photodynamic therapy by a dual-stage light irradiation strategy. When the micelles were accumulated in tumor tissues, the first light irradiation (L_1, 6 min) was utilized to facilitate cellular uptake by "photochemical internalization" (PCI). Then the intracellular glutathione (GSH) would induce the PTX release, micelles disassembly and the aggregation state change of AIEgens. The fluorescence signal change of two AIEgens-based ratiometric fluorescent probe could not only precisely guide the second light irradiation (L_2, 18 min) for sufficient ROS production, but also monitor the non-fluorescent drug PTX release in turn. Both *in vivo* and *in vitro* studies demonstrated that the dual-stage light irradiation strategy employed for TB@PMPT micelles exhibited superior therapeutic effect than only 24-min continuous light irradiation.

KEYWORDS: AIEgen-based photosensitizer, dual-stage light irradiation strategy, ratiometric fluorescent probe, improved cellular uptake, combined chemo-photodynamic therapy.

For photodynamic therapy (PDT), photosensitizers play an important role in generating reactive oxygen species (ROS), therefore their intracellular behaviors could greatly influence the therapeutic effect.[1] For example, numerous conventional photosensitizers with extended π conjugation, such as porphyrins and their derivatives, could effectively emit fluorescence signal and conduct photodynamic reaction in molecular-dissolved state, but their emission as well as ROS producing ability would be attenuated in aggregation state, which is caused by aggregation-caused quenching (ACQ). It significantly hampers the application of PDT, especially the fluorescence image-guided PDT. Recently, aggregation-induced emission (AIE) photosensitizers show their superiority and strong potential. They are nearly non-emissive in molecular-dissolved state, but display strong emission when aggregated due to the restriction of intramolecular motions.[2-5] AIE photosensitizers are able to show both high fluorescence and efficient photosensitization in the aggregate state.[6-9] Moreover, the dynamic fluorescence transformation of aggregation-induced emission luminogens (AIEgens) under different circumstances is intriguing and significant, because it could be used to reflect the specific stimuli in tumor environment and monitor the structure changes of nanocarrier.[10-13] Though delightful developments, the anti-tumor efficiency of AIEgen-based PDT is not as good as expected and still far away from clinical applications due to the unsatisfying therapeutic efficiency.

Combinational therapy that integrates different therapeutic modalities provides an opportunity to achieve better therapeutic efficacy and decreased side effects.[14-17] For instance, when combined with chemotherapy, PDT not only enhances the immune

response by triggering acute inflammation and leukocyte infiltration, but also relieves tumor cell resistance to chemotherapeutic drug. However, the limited cellular internalization of drug delivery systems would severely restrict the efficacy of combined chemo-photodynamic therapy. Though tremendous efforts have been devoted to enhancing cellular uptake, such as grafting target parts,[18, 19] changing the morphology,[20-22] and reducing the size,[23, 24] synthesis methods are extremely complex to endow nanocarriers with the above functions. Encouragingly, cellular uptake efficiency of nanocarriers can also be improved by the "photochemical internalization" (PCI) effect. Through a short-time light irradiation, a small amount of ROS produced by photosensitizer could induce lipid peroxidation and increase cell membrane permeability, leading to enhanced intracellular internalization.[25-30] After uptake by tumor cells, abundant ROS produced under the second light irradiation and the released chemotherapeutic drugs would play their respective roles in the cytoplasm and kill tumor cells. However, the second light irradiation occasion is hard to decide. The strategy of "stimuli-triggered imaging" based on the specific tumor microenvironment are adopted to realize visualization and choose the appropriate irradiation occasion for performing PDT, such as ratiometric fluorescence imaging.[26, 31, 32] Even so, these traditional fluorescent dyes show no additional functions except for providing fluorescent signals in the system. The introduction of too many fluorescent dyes reduces the proportion of drugs and results in an increased metabolic burden, although many of which are biocompatible. Therefore, AIE photosensitizers used as excellent theranostic fluorescent dyes to construct ratiometric fluorescence imaging technique may guide the

second light irradiation occasion precisely. That is to say, combining dual-stage light irradiation strategy with ratiometric fluorescence imaging based on AIE photosensitizer helps to improve the tumor suppressing efficacy of combined chemo-photodynamic therapy.

To overcome the limited cellular uptake efficiency of nanocarriers and to adopt the optimal irradiation occasion for PDT, in this study, a self-guiding polymeric micelle with two AIE photosensitizers and a reduction-sensitive paclitaxel prodrug (PTX-SS-N_3) was established for enhancing chemo-photodynamic therapy by the dual-stage light irradiation strategy. As shown in Scheme 1, AIE photosensitizer PyTPE and anticancer drug paclitaxel (PTX) were conjugated on backbone of amphiphilic polycarbonate to obtain the reduction-sensitive polymeric prodrug PEG-*b*-PMPMC-*g*-PTX-*g*-PyTPE (PMPT) by azide-alkyne CuAAC click reaction. Then, another AIE photosensitizer TPA-BDTP (TB) was entrapped into hydrophobic core of PMPT micelles to prepare TB@PMPT micelles. The TB@PMPT micelles could emit both yellow fluorescence from PyTPE and red fluorescence from TB. When micelles reached the tumor tissue, the ROS produced by PyTPE and TB under the first light irradiation (L_1) can induce lipid peroxidation and increase the permeability of cell membrane, resulting in improved cell uptake of TB@PMPT micelles. Then, the intracellular high concentration of glutathione (GSH) can crack the disulfide bond in PMPT chains and achieve the controlled release of PTX in the cytoplasm. Subsequently, increasing the hydrophilicity of the residual polymer could improve the dispersion of PyTPE in aqueous solution, while hydrophobic TB remains aggregated without change, which

would lead to the fluorescence ratio transformation. That is to say, the photosensitizers PyTPE and TB in micelles can also be used as built-in ratiometric fluorescent probe to precisely guide the occasion for second irradiation to achieve PDT. Reasonable utilization of dual-stage light irradiation strategy and excellent design of AIEgen-based ratiometric fluorescent probes are expected to improve the efficacy of combined chemo-photodynamic therapy eventually.

RESULTS AND DISCUSSION

ROS produced under the first light irradiation (L_1) improves the cellular internalization of TB@PMPT by PCI effect.

To obtain the reduction-sensitive amphiphilic polymeric prodrug PEG-*b*-PMPMC-*g*-PTX-*g*-PyTPE (PMPT), the PTX prodrug (PTX-SS-N_3) and AIE photosensitizer of PyTPE were anchored on the amphiphilic block polymer PEG-*b*-PMPMC (PM) through azide-alkyne CuAAC click reaction (Figure S1). PTX-SS-N_3, PyTPE and PM were synthesized according to our previous work.[33, 34] The relative characterizations are shown in Figure S2-S7 and consistent with the literatures. As revealed by ^{1}H NMR (Figure S8), PMPT has average 2.2 units of PTX groups and 1.1 units of PyTPE groups on the polycarbonate backbone. Gel permeation chromatography displayed a unimodal distribution at an elution time of 22.7 min, confirming successful synthesis of PMPT (Figure S9). Another AIE photosensitizer of TB was synthesized according to the literature.[7] The AIE photosensitizers of PyTPE and TB not only possess satisfactory ROS yields under light irradiation in aqueous solution, but also have good photostability and photobleaching resistance in its nanoaggregates, which makes them

suitable for image-guided PDT.[34-36] TB@PM, TB@PMP and TB@PMPT micelles were obtained by self-assembling of amphiphilic polymer micelles and TB. The hydrodynamic sizes of TB@PM and TB@PMP micelles were 60.2 ± 1.5 nm (PDI = 0.121 ± 0.016) and 73.4 ± 2.3 (PDI = 0.143 ± 0.015) (Table S1). TB@PMPT micelles with TB loading of 7.57%, 9.57%, and 10.8% were prepared by controlling feed ratio (Table S1). When the loading contents of TB was 9.57%, the transmission electron microscopy (TEM) images confirmed that PMPT and TB@PMPT micelles were uniform spherical shape (Figure S10A and S10B). The hydrodynamic sizes of PMPT and TB@PMPT were 116.8 ± 2.5 nm (PDI = 0.142 ± 0.017) and 132.9 ± 1.6 nm (PDI = 0.120 ± 0.047), respectively (Figure S11A and Table S1). PMPT and TB@PMPT micelles exhibited excellent stability at room temperature (Figure S10C, S10D and S11B). TB@PMPT micelles displayed strong absorption peak at 400 nm and 530 nm, which was attributed to PyTPE and TB, respectively (Figure S12). PMPT micelles showed strong fluorescence signal at 583 nm and negligible signal at 684 nm at the excitation wavelength (Ex) of 400 nm, and TB@PMPT micelles exhibited weak signals at 583 nm and strong signal at 684 nm at the Ex of 530 nm, respectively, which illustrated that the interference between the PyTPE and TB fluorescence signals was negligible and ensured the potential of PyTPE and TB serving as a ratiometric biosensor (Figure S13).

To demonstrate the ROS production capacity of AIE photosensitizers of PyTPE and TB for TB@PMPT micelles, 9,10-anthracenediyl-bis(methylene)dimalonic acid (ABDA) and 2′,7′-dichlorofluorescin diacetate (DCFH-DA) were used as indicators in

aqueous solution and tumor cell environment respectively. The peak of 378 nm of ABDA in TB@PMP, PMPT and TB@PMPT micelles decreased during irradiation, whether these samples have been pretreated with 10 mM DL-dithiothreitol (DTT) (Figure S14). The decomposition rate curves of ABDA generated by ROS from these micelles samples were shown in Figure 1A. The slopes of decomposition curves of these micelles were calculated to be 0.07347 ± 0.00190, 0.08902 ± 0.00198, 0.11750 ± 0.00244, 0.08153 ± 0.00236, 0.04521 ± 0.00028 and 0.08811 ± 0.00237 for TB@PMP, PMPT, TB@PMPT and their micelles pretreated with 10 mM DTT for 1 h, respectively (Table S2). Obviously, TB@PMPT micelles with two AIE photosensitizers have better ROS generation capacity than PMPT and TB@PMP micelles with only one AIEgen photosensitizer. Compared with the PMPT micelles pretreated by DTT, PMPT micelles without any treatment exhibited better ROS generation capacity, proving that the dissociation of PTX enhances the hydrophilicity of the residual polymer, contributes to the dispersion of PyTPE in the aqueous solution, and therefore results in a decrease in the ROS production. In the cell sample, bright green fluorescence signal was found for the group of HeLa cells treated with TB@PMP, PMPT and TB@PMPT micelles with white light irradiation, while negligible green fluorescence signal was found for the groups without light irradiation (Figure 1B and S15). Also, PMPT and TB@PMPT micelles have better ROS generation capacity than corresponding DTT-treated micelles, which was consistent with ROS generation in aqueous solution (Figure S16). The above results showed that TB@PMPT micelles possessed satisfactory ROS generation efficiency in aqueous solution and in HeLa cells.

To demonstrate enhanced cell uptake by PCI effect, the cellular internalization of TB@PM and TB@PMPT micelles was studied by confocal laser scanning microscopy (CLSM) under short light irradiation. The fluorescence of TB from TB@PM and TB@PMPT micelles are mainly distributed in the cytoplasm (Figure S17). When HeLa cells received the first light irradiation (L_1, 6 min), the observed red fluorescent region was larger than that of the cells without light irradiation for TB@PM and TB@PMPT micelles, which indicated that the cell uptake of the micelles can be enhanced by the first light irradiation (Figure 1C). In addition, the mean fluorescence intensity (MFI) of cells treated with TB@PMPT (L_1) was about 1.4 times higher than that of TB@PM (L_1) (Figure 1D). The reason may be that TB@PMPT micelles with two AIE photosensitizers have better ROS production efficiency than TB@PM micelles with only one AIEgen photosensitizer, leading to enhanced cell uptake of micelles by PCI effect. Besides, the ability of nanoparticles to escape from lysosomes can be enhanced by photochemical disruption of endocytic membranes. The correlation between green (lysosomes) and red (TB) fluorescence was evaluated by Pearson's correlation coefficients (R_r).[37, 38] The magnitude of the R_r value represents the probability that two molecules will appear in the same space. With or without light irradiation (L_1), the R_r values of the green and red fluorescence for TB@PMPT micelles were 0.17 and 0.49, respectively, which indicates that the escape of TB can be facilitated under the short light conditions (Figure 1E). Moreover, TB@PM micelles had no obvious toxicity to HeLa cells regardless of irradiation when TB concentration was 4.79 and 7.20 μg mL^{-1}, respectively, but the cell viability of TB@PMP micelles decreased after light

irradiation at the same TB concentration (Figure 1F and 1G). Also, the cellular internalization of TB@PMPT by different time irradiation (L_1) was evaluate. As shown in Figure S18, the red fluorescent intensity of TB enhanced with the increase of light time. After irradiation for 2, 4 and 6 minutes, the fluorescence intensity was about 1.3, 1.7 and 2.1 times higher than that without irradiation, respectively. So, 6-min was determined as the time for the first short light irradiation. These results together illustrated that TB and PyTPE as AIE photosensitizer could enhance the uptake by cells, promote the escape of the micelles through the PCI effect under the first light irradiation, and subsequently improve the efficacy of combined chemo-photodynamic therapy.

A ratiometric fluorescence imaging probe was constructed based on AIEgens under the reductive intracellular environment.

Glutathione (GSH), a γ-glutamyl-cysteinyl-glycine tripeptide capable of reducing disulfide bonds, is the most abundant biological reducing agent in tumor cell cytoplasm (2-10 mM) but rarely present in plasma (~2 μM).[39] Compared with normal tissues, tumor tissues possess a high reducing potential with at least a 4-fold higher GSH concentration. Therefore, amphiphilic copolymers or polymer prodrugs incorporated disulfide bonds are stable under oxidizing conditions, but cleavable in a reducing environment. In order to investigate the redox-responsive of polymer prodrug of PMPT in response to the redox trigger (Figure 2A). The release product from the prodrug PTX-SS-N_3 under the condition of 10 mM DTT was first evaluated by high performance liquid chromatography (HPLC) and high resolution mass spectrometry (HRMS). As

shown in Figure 2B, PTX, PTX-SH and PTX-SS-N_3 exhibited monodisperse peak at elution time of 7.26, 13.3 and 25.0 min, respectively. After incubation of PTX-SS-N_3 with 10 mM DTT, two new peaks belonged to PTX and PTX-SH appeared at elution time of 7.29 and 13.3 min, respectively, suggesting that the active PTX can be rapidly released by crack the disulfide bond. Then the collected PTX-SH was reanalyzed by HPLC and HRMS, and a peak belonged to PTX at elution time of 7.26 min was still observed, illustrating that the conversion from PTX-SH to PTX occurred rapidly. In addition, the peaks of PTX, PTX-SH and 3-mercaptopropanoic acid was also observed from HRMS (Figure S19). Thus, the conversion process of PTX-SH was proposed as shown in Figure S20 that PTX can be released after the ester moiety undergoes an intramolecular nucleophilic acyl substitution of the free thiol group. Then, to demonstrate the effect of reducing agents on the release of prodrug PMPT micelles (Figure 2A), the critical micelle concentrations (CMC) of PMPT micelles at different DTT concentrations were compared to assess the disintegration of reduction-sensitive PMPT micelles. The CMC value of PMPT micelles was 3.39 mg L^{-1}, and the CMC values of PMPT micelles were 16.9, 54.7 and 139 mg L^{-1} after pretreated with 2, 10 and 50 mM DTT for 1 h, respectively (Figure S21). The increase of CMC value was attributed to increased hydrophilic of the residual polymer by the cleavage of disulfide bonds under reducing conditions.[40] In addition, after incubation of TB@PMPT micelles with 10 mM DTT, peaks of PTX (7.26 min) and PTX-SH (13.3 min) were observed by HPLC (Figure 2B), and the mass spectrum peaks of PTX, PTX-SH, 3-mercaptopropanoic acid and TB were also observed by HRMS (Figure S22).

Furthermore, due to the cleavage of disulfide bonds under reducing conditions, the micelles structure might be unstable. As seen in Figure S23, the PMPT and TB@PMPT micelles became quite chaotic in size upon incubation with DTT and aggregates with a hydrodynamic size were observed. The changed size was attributed to the transition from hydrophobicity to hydrophilicity under reducing conditions.

The influence of intracellular micro-reducing environment on the release behavior of conjugated PTX from PMPT micelles has also been investigated, 10 mM GSH was performed to simulate the reducing environment of cytoplasm *in vitro* to study the reduction-triggered transition of PMPT micelles that possessed disulfide linkages positioned in the joints between PTX and the polycarbonate backbone. The accumulative drug release profiles as a function of time are plotted in Figure 2C, the higher concentration was, the faster the drug was released. For example, without or at a GSH concentration of 10 μM, less than 5% of paclitaxel was released from PMPT within 12 hours. While 31% of PTX was released at a GSH concentration of 2 mM and 46% was released at a GSH concentration of 10 mM in the same time period. These results indicated that the disulfide bonds of the PMPT could be cleaved by GSH efficiently to produce thiol groups, PTX can be released after the ester moiety undergoes an intramolecular nucleophilic acyl substitution of the free thiol group and form a hydroxyl group on the residual polymer segment in aqueous solution.[41]

To investigate whether PTX can be released from TB@PMPT micelles under the reducing microenvironment of cytoplasm of tumor cells or not, cell extract after incubation of TB@PMPT micelles with HeLa cells was analyzed by HRMS (Figure

2D). As shown in Figure S24, the mass spectra peaks of PTX-SH, PTX, 3-mercaptopropanoic acid and TB were also observed. This demonstrated that TB@PMPT micelles can be efficiently uptaken by tumor cells and release PTX efficiently. Furthermore, intracellular PTX and PTX-SH were monitored by HPLC after HeLa cells were incubated with TB@PMPT micelles for different times. PTX-SH and PTX were observed simultaneously at different durations. The quantitative statistics of the PTX-SH and PTX in the cells was shown in Figure 2E. The sum of the peak areas of PTX-SH and PTX increased with time, and increased to 5.6 times after 7 h, indicating that PTX can be released from micelles in the cytoplasm and the amount of drug released increases with time.

The detachment of PTX from PMPT under the reducing environment could enhance the hydrophilicity of the residual polymer and affect the aggregation morphology and fluorescence signal of PyTPE from PMPT micelles. The fluorescence spectra of PMPT micelles were measured after incubated with 10 mM DTT. With time elapsing, the fluorescence of PyTPE decreased very rapidly when PMPT micelles with different concentrations were incubated with 10 mM DTT (Figure S25 and S26). The fluorescence could drop by about 80 times after 8 h. The rapid fluorescence decreases of PyTPE might be attributed to the fact that the enhanced hydrophilicity of the residual polymer by the detachment of PTX and the formation of hydroxyl groups. The hydrophilic PEG segment of residual polymer would contribute to the dispersion of PyTPE in the aqueous solution. Then, the enhanced hydrophilicity significantly promoted the free rotation of phenyl, leading to the aggregation-induced emission

decline of PyTPE. Fluorescence intensity of TB@PMP micelles was not found to change significantly for 30 h under the reduction condition of 10 mM DTT in our previous study.[36] Furthermore, the ratio of fluorescence intensity between TB and PyTPE (I_{TB}/I_{PyTPE}) was studied when TB@PMPT micelles with different concentration and different TB loading (7.57%, 9.57% and 10.8%) were incubated with 10 mM DTT. There is no obvious decrease for fluorescence intensity of TB (Ex = 530 nm) within 24 h, because it remains aggregated in aqueous solution, regardless of whether it is loaded or released from the micelles (Figure S27). In addition, the fluorescence of PyTPE (Ex = 400 nm) decreased rapidly, which was similar to that of PMPT micelles. It is important that the ratio of I_{TB}/I_{PyTPE} becomes larger than 80 times after 8 hours for TB@PMPT micelles (Figure 2F). Obviously, this ratiometric fluorescence biosensor based polymeric prodrug TB@PMPT micelles exhibited great advantages in identifying the reducing environment by the detachment of PTX, which can be used to guide appropriate irradiation occasion for performing PDT in reducing tumor cytoplasmic environment. Encouraged by the satisfactory redox-induced fluorescence changes in TB@PMPT micelles, the feasibility of using the ratiometric fluorescence biosensor in living cells was assessed. After incubation of HeLa cells with PMPT and TB@PMPT micelles, the fluorescence signals of TB and PyTPE were recorded by CLSM. As shown in Figure S28A, after incubated with HeLa cells, PMPT micelles showed gradually decreased yellow signal, and after incubation for 7 h, the fluorescence signal intensity decreased by about 9 times of the initial value. The fluorescent signal of PyTPE in HeLa cells was further verified by the addition of GSH-OEt and BSO,

which were used as external enhancers/reductants to regulate intracellular GSH concentration.[42] The results showed that the addition of GSH could promote the decrease of yellow signal, and the addition of BSO could inhibit the decrease of yellow signal, indicating that the decrease of yellow signal is related to GSH concentration (Figure S28B, S28C and S28D). Regardless of whether the HeLa cells were pretreated with GSH-OEt or BSO, the yellow fluorescent signal of PyTPE of TB@PMPT micelles has a similar trend to that of the corresponding PMPT micelles (Figure 2G, 2H, S29 and S30). It is worth noting that there was almost no difference in the signal intensity of TB in HeLa cells pretreated with or without GSH-OEt or BSO. This shows that TB could act as a fluorescent internal reference material for ratiometric fluorescent. These results indicated that GSH secreted by tumor cells detached PTX from TB@PMPT micelles, leading to decrease of fluorescence signal of PyTPE, while the fluorescence signal of TB remains stable, which can be used to guide appropriate irradiation occasion for performing PDT in living cells.

***In vitro* therapeutic efficacy of TB@PMPT by dual-stage light irradiation strategy.**

As we known, the decomposition of microtubules and induce apoptosis can be enhanced by PTX.[43] The effect of PMPT micelles on the microtubule integrity of HeLa cells was recorded by CLSM using anti-α-tubulin-FITC antibody as indicator. After incubation with PM micelles, no significant morphological change was observed in the microtubules of HeLa cells (Figure 3A). However, the microtubules of the cells were contracted and damaged after incubated with PMPT for 8 h and 16 h, which can be attributed to that the release of PTX promotes the assembly of tubulins and prevents

them from depolymerization, resulting in replication failure and apoptosis of HeLa cells.

Furthermore, we expect the dual-stage light irradiation strategy based on the integration of PCI to improve the tumor suppression efficacy by combined chemo-photodynamic therapy. To confirm this speculation, CCK-8 assay was performed on HeLa cells to assess cytotoxicity of TB@PMPT micelles under the dual-stage light irradiation, that is, a first light irradiation (L_1, 6 min) during cellular internalization, followed by the second-time light irradiation (L_2, 18 min) after cellular internalization. TB@PM, PMPT and TB@PMPT micelles under only 24-min continuous light irradiation (LL) for the second light irradiation was determined as the control. First, negligible cytotoxicity was observed of light irradiation (white light, 70 mW cm^{-2}) with only 24 min (LL) and dual-stage light irradiation (L_1L_2) on HeLa cells (Figure S31). In addition, significant cytotoxicity was observed for TB@PM, PMPT and TB@PMPT micelles received only 24-min irradiation (LL). The cytotoxicity was further enhanced when the dual-stage light irradiation strategy (L_1L_2) was employed (Figure 3B-E). Considering that both ROS and PTX could inhibit tumor growth, the synergetic efficacy of TB@PMPT micelles between TB and PMPT with light irradiation against HeLa cells was evaluated by CCK-8 assay. Our previous studies have shown that the dark toxicity of AIE photosensitizer of TB is negligible, and the influence of light irradiation on the toxicity of polymer prodrug PTX is negligible. Also, there was no significant cytotoxicity difference between PMPT (-) and TB@PMPT (-) without light irradiation

toward HeLa cells, free PTX (-) showed more efficient cell-growth inhibition than PMPT (-) and TB@PMPT (-) (Figure S32).

TB@PMPT (LL) showed enhanced cytotoxicity compared to PMPT (LL) and TB@PM (LL), and TB@PMPT (L_1L_2) also showed enhanced cytotoxicity compared to PMPT (L_1L_2) and TB@PM (L_1L_2). The above results demonstrate that this co-delivery micelles system shows a stronger therapeutic effect when the strategy of dual-stage light irradiation was performed. In addition, regardless of whether the dual-stage light irradiation strategy was implemented, compared with the sum of PMPT and TB@PM group individually at the same PTX, TB, and PyTPE concentrations, it was found that the cell inhibition ratio was greater for TB@PMPT (green bar) (Figure 3F, S33, and S34). TB@PMPT micelles exhibited effective inhibition of tumor cells due to the combination of enhanced chemotherapy and PDT. Therefore, this system demonstrated that the PCI of AIEgen photosensitizer under the first light irradiation improved the cellular internalization of TB@PMPT micelles. Subsequently, PTX could release from polymeric prodrug in the cytoplasm to promote the decomposition of microtubules. Consequently, generation of ROS in tumor cells under the second light irradiation also induce tumor cells apoptosis to enhance the efficacy of combined chemo-photodynamic therapy effectively. Moreover, the cell morphology was studied by bio-TEM after treated with TB@PMPT (-), TB@PMPT (LL) and TB@PMPT (L_1L_2) respectively. As shown in Figure 3G, because of the release of PTX and ROS from AIE photosensitizers, the mitochondria and nuclear membrane with different destructive forms can be observed. The results showed that increased cellular uptake

and cytotoxicity of micelles can be achieved through improved membrane permeability.

***In vivo* imaging and combinational therapy efficacy.**

Biocompatibility of polymeric prodrug micelles of PMPT and TB@PMPT were evaluated by hemocompatibility assays prior to *in vivo* application. As shown in Figure S35, hemolysis was less than 5% at all micelle concentrations ranging from 62.5 to 2000 mg mL^{-1}. Similarly, no morphological change of erythrocytes was observed in the PMPT and TB@PMPT micelles at the concentration up to 2000 mg mL^{-1}, while erythrocyte lysis occurred in the positive control (Figure S36). This indicates that the polymeric prodrug micelles are blood compatible and can be administered intravenously for *in vivo* applications. Then, the *in vivo* biodistribution of the TB@PMPT micelles was studied by using HeLa tumor-bearing nude mice. TB and PyTPE in TB@PMPT micelles were traced by utilizing a small animal imaging system. It was found that TB@PMPT micelles gradually accumulated in tumor tissue and reached a maximum within 8 h (Figure 4A). The fluorescence intensity of TB in tumor tissue is much higher than that of PyTPE, which may be due to the higher permeability of TB fluorescence in biological tissue. Fluorescence signal of TB and PyTPE in the tumor decreased over time due to drug metabolism, but TB fluorescence was still observed after 24 h after injection. Meanwhile, the distribution of TB@PMPT micelles within 24 h was studied by comparing the fluorescence distribution of TB and PyTPE in tumor and other organs. As shown in Figure 4B, strong fluorescence for TB and PyTPE was observed in the tumor tissue, weak fluorescence was observed in the liver,

and almost no fluorescence was observed for the spleen, lung, kidney, and heart. Figure 4C showed the average fluorescence signal of TB and PyTPE in tumors and organs. These results suggest that TB@PMPT micelles can be selectively accumulate in tumor tissue *via* enhanced permeability and retention (EPR) effect.[44] To evaluate the *in vivo* anti-tumor efficacy of the TB@PMPT micelles (L_1L_2), HeLa tumor-bearing nude mice were *i.v.* injected with different materials. PBS (-), TB@PMPT (-) and TB@PMPT (LL) were employed as the controls, the anti-tumor efficacy of TB@PMPT micelles was shown in Figure 4D-F. Compared with the group of PBS (-) and TB@PMPT (-), tumor growth was significantly inhibited after intravenous injection of TB@PMPT micelles with light irradiation. Especially, the tumor inhibition rate of mice treated with TB@PMPT (L_1L_2) was higher than that of mice treated with TB@PMPT (LL), after 12 days of treatment, the relative volume of treated tumors in TB@PMPT (L_1L_2) group was smaller than that in the control group. Weight measurement is used to evaluate the systemic toxicity. When mice were treated with TB@PMPT micelles during treatment, the change in body weight was negligible (Figure S37), indicating that the systemic toxicity of TB@PMPT micelles is very weak. Furthermore, hematoxylin and eosin (H&E) assays were used to analyze the organs and tumors in each group after 12 days of administration. As shown in Figure S38, compared with PBS group, no detectable phenomenon of inflammation or tissue damage was found in heart, liver, lung, spleen, and kidney. TB@PMPT (L_1L_2) micelles group presented significant nuclear condensation and fragmentation, implying that the dual-stage light irradiation strategy could enhance the combined chemo-photodynamic therapy effect.

CONCLUSIONS

In summary, we presented a self-guiding polymeric micelle of TB@PMPT consisting of two AIE photosensitizers and a reduction-sensitive PTX prodrug to enhance combined chemo-photodynamic therapy by the dual-stage light irradiation strategy. TB@PMPT micelles exhibited strong emission in both yellow fluorescence of PyTPE and red fluorescence of TB, and performed well in ROS generation. The AIE photosensitizer could not only enhance the cellular internalization of the TB@PMPT micelles under the first light irradiation by PCI effect, PyTPE and TB can also be used as ratiometric fluorescent probe to guide the second light irradiation in cytoplasm and monitor the non-fluorescent drug release. Combing the sufficient ROS generation under the second light irradiation with GSH responsive release of PTX in the cytoplasm could achieve an enhanced chemo-photodynamic therapy. The design of nanosystem and the utilization of irradiation strategy could inspire more valuable idea to overcome the obstacles in combination therapy.

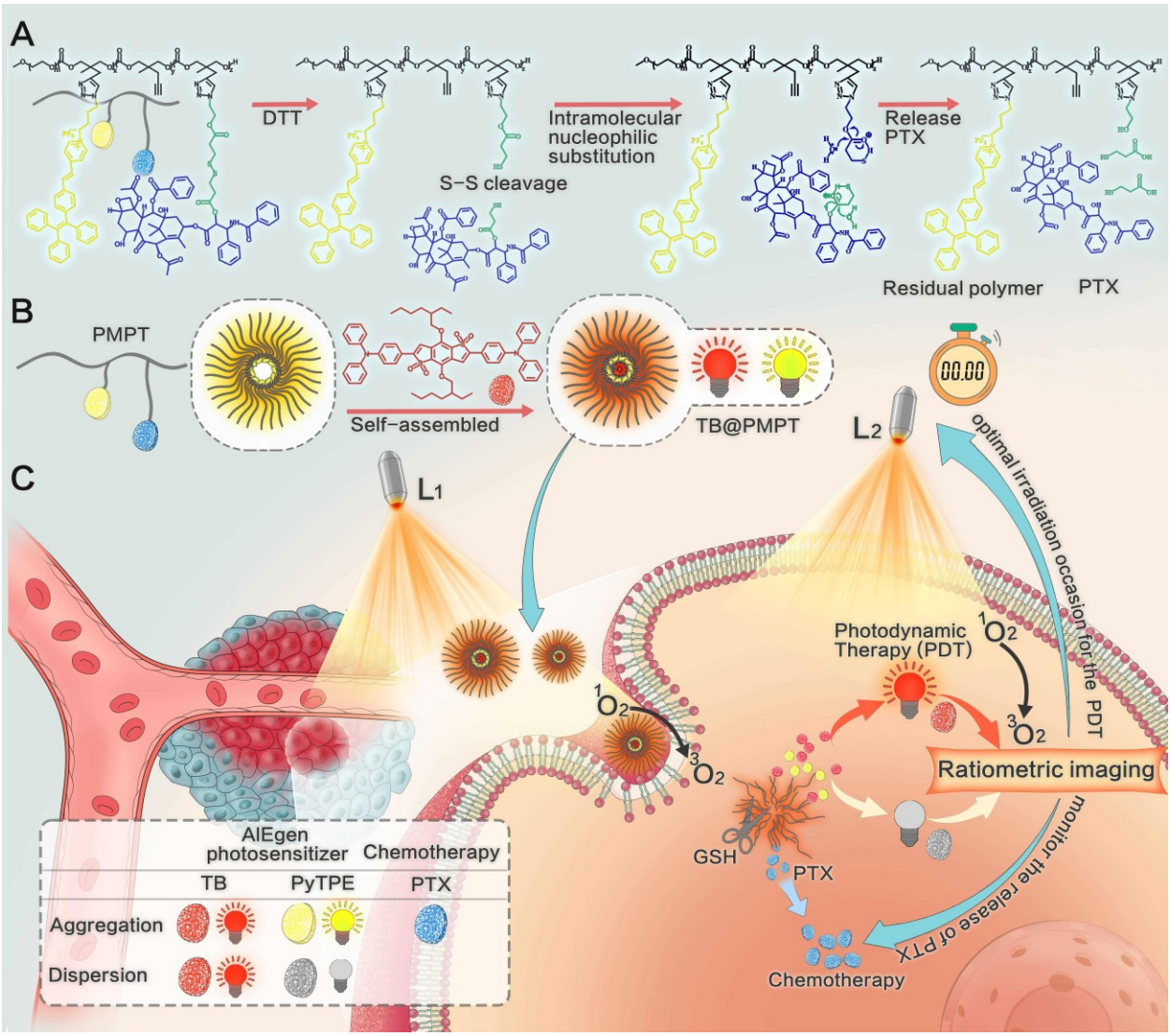

Scheme 1. A self-guiding polymeric prodrug micelle composed of two AIE photosensitizers (PyTPE and TB) was developed for guiding PDT precisely and monitoring the release of PTX into one single platform for enhanced combined chemo-photodynamic therapy by dual-stage light irradiation strategy. (A) The mechanism of PTX release from polymeric prodrug PMPT under the reducing environment. (B) The amphiphilic polymer PMPT can be self-assembled into micelles, and TB@PMPT micelles were prepare by encapsulate the hydrophobic AIEgen TB through hydrophobic interaction. (C) When the TB@PMPT micelles were accumulated in tumor tissues, the first light irradiation (L_1) was utilized to facilitate cellular uptake by

“PCI”. Then the intracellular GSH would induce the PTX release, micelles disassembly and the aggregation state change of AIEgens. The specific imaging of two AIEgens-based ratiometric fluorescent probe could precisely guide the second light irradiation (L_2) for sufficient ROS production and monitor the non-fluorescent drug PTX release for chemotherapy

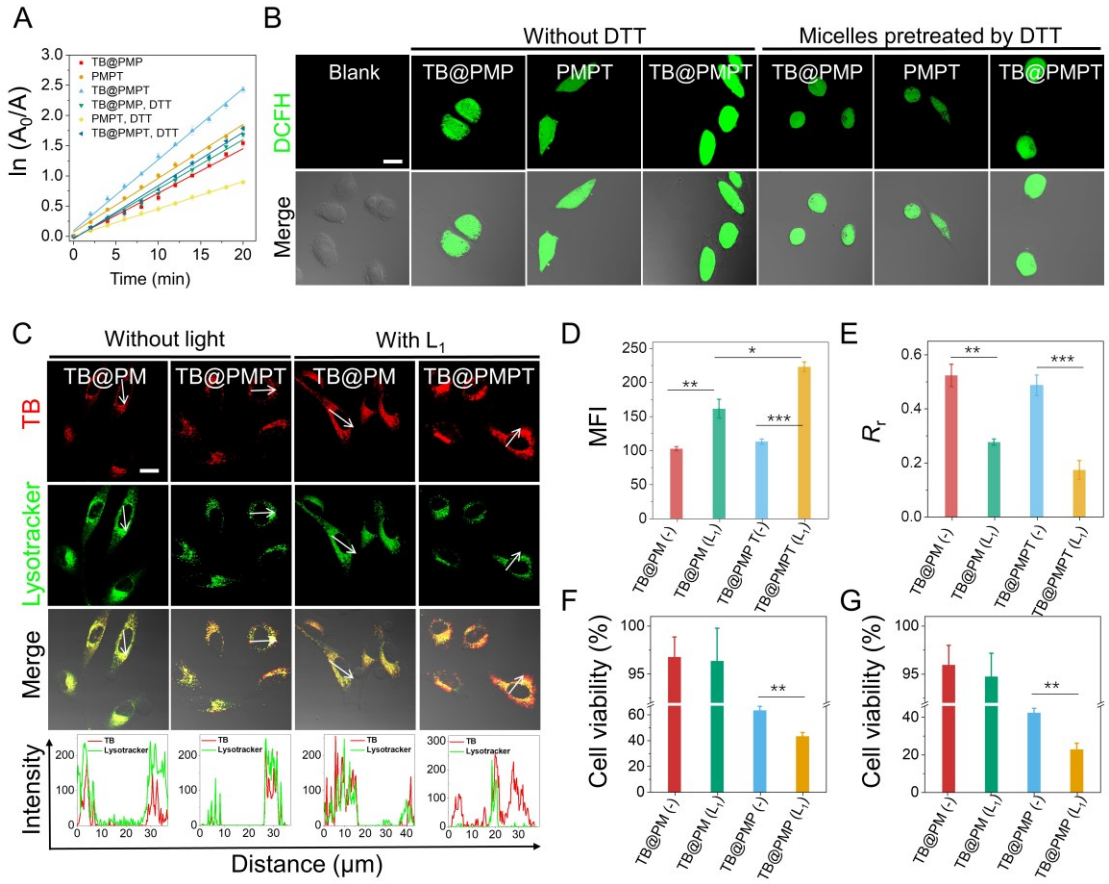

Figure 1. ROS produced under the first light irradiation improves the cellular internalization of TB@PMPT by PCI effect. (A) Decomposition rates of ABDA, which was induced by ROS that was generated from TB@PMP, PMPT and TB@PMPT with or without 10 mM DTT treatment at 37 °C for 1 h, were studied. (B) Detection of intracellular ROS production by DCFH-DA in HeLa cells after incubation with TB@PMP, PMPT and TB@PMPT micelles with or without 10 mM DTT were pre-incubated at 37 °C for 1 h under light irradiation (6 min, white light, 70 mW cm^{-2}). (C) CLSM images of HeLa cells and corresponding colocalization analysis after incubation with TB@PM and TB@PMPT micelles with or without the first light irradiation (L_1). (D) Corresponding quantitative analysis of the fluorescence intensity of TB in CLSM

images by the Zeiss LSM 880 software. (E) Pearson's correlation coefficient of the red/green fluorescence which in confocal images. (F and G) CCK-8 assay of TB@PM and TB@PMP in HeLa cells after incubation for 48 h (L_1: samples received 6-min light irradiation, white light, 70 mW cm^{-2}; F: $C_{TB@PM}$ = 66 μg mL^{-1}, $C_{TB@PMP}$ = 51 μg mL^{-1}, C_{TB} = 4.79 μg mL^{-1}; G: $C_{TB@PM}$ = 99 μg mL^{-1}, $C_{TB@PMP}$ = 77 μg mL^{-1}, C_{TB} = 7.20 μg mL^{-1}). Scale bar: 20 μm. Data was reported as mean ± SD and analyzed through two-sided Student's *t*-test. (***$p < 0.001$, **$p < 0.01$, *$p < 0.05$)

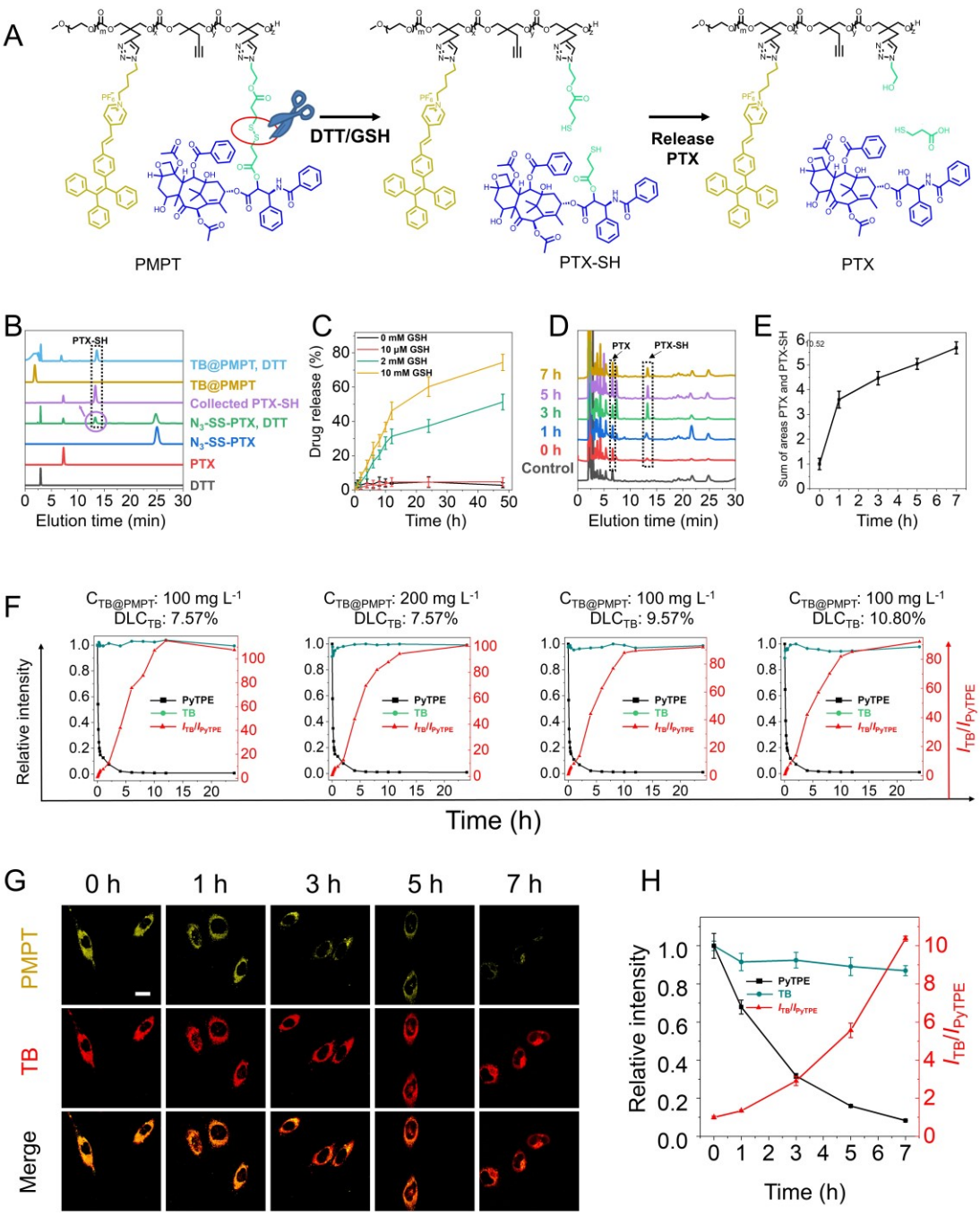

Figure 2. Reductive intracellular environment induces the release of PTX, disassembly of micelles and the aggregation state change of AIEgens. (A) The release mechanism of free PTX from PMPT under the reducing environment. (B) HPLC analysis to detect the PTX release of prodrug PTX-SS-N_3 and TB@PMPT micelles under the condition of 10 mM DTT. (C) Drug release from PMPT micelles in PBS (pH 7.4, 0.1 M) containing 0.1% (w/v) Tween 80 at 37℃ with different concentration of GSH. (D)

HPLC analysis of drug release of PTX and PTX-SH from TB@PMPT micelles in the HeLa cells. (E) Quantitative analysis of the sum of the peak areas of PTX-SH and PTX in cells by HPLC. (F) Fluorescence (FL) intensity of TB, PyTPE and I_{TB}/I_{PyTPE} of TB@PMPT micelles with different concentrations and different TB loading amounts incubated with 10 mM DTT for different times. (PyTPE: Ex = 400 nm, Em = 583 nm; TB: Ex = 530 nm, Em = 684 nm). (G) Fluorescence change of TB@PMPT micelles was incubated with HeLa cells for 2 h. (H) Quantitative analysis of the fluorescence intensity of PyTPE and TB and quantitative analysis of I_{TB}/I_{PyTPE}. PyTPE: yellow signal, Ex = 405 nm; TB: red signal, Ex = 543 nm.

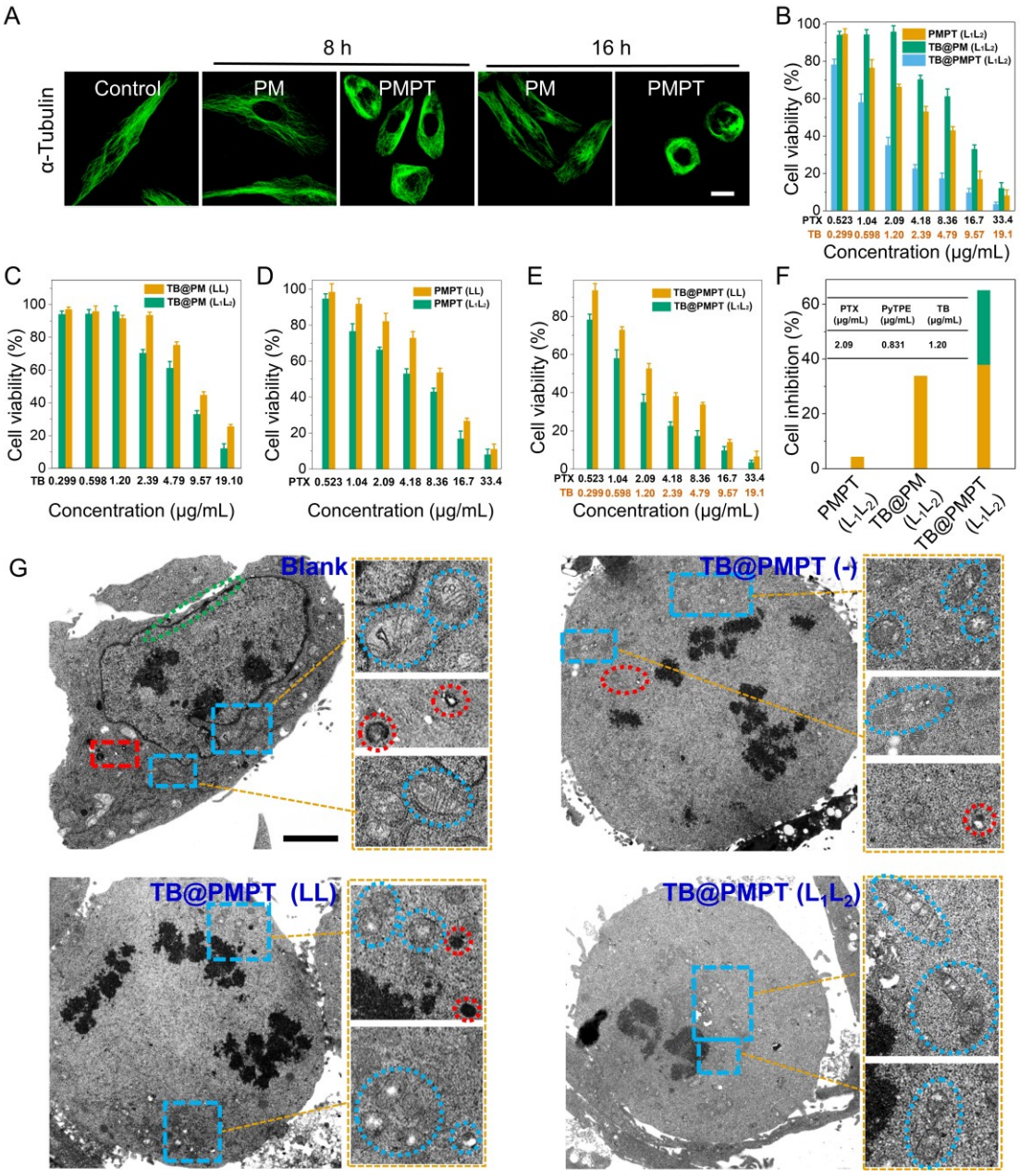

Figure 3. *In vitro* therapeutic efficacy of TB@PMPT. (A) Detection of microtubules in HeLa cells after incubated with PM and PMPT micelles for 8 and 16 h, respectively. (B-E) CCK-8 assay of TB@PM (LL) and TB@PM (L_1L_2), PMPT (LL) and PMPT (L_1L_2), TB@PMPT (LL) and TB@PMPT (L_1L_2) in HeLa cells after incubation for 48 h (LL: samples received 24-min continuous irradiation; L_1L_2: samples received dual-stage light irradiation, 6-min for L_1 and 18-min for L_2, white light, 70 mW cm^{-2}). (F) The inhibition ratios of TB@PM (L_1L_2), PMPT (L_1L_2), and TB@PMPT (L_1L_2) micelles

treated cells upon light irradiation (white light, 70 mW cm^{-2}), respectively. The green bar denotes the additional cell inhibition ratio gained when TB@PMPT (L_1L_2) are combined, compared with the sum of TB@PM (L_1L_2), PMPT (L_1L_2). (G) Bio-TEM images of HeLa cells treated with TB@PMPT (-), TB@PMPT (LL) and TB@PMPT (L_1L_2), respectively. Nuclear membrane, mitochondria and lysosome are highlighted by green, blue and red circles, respectively.

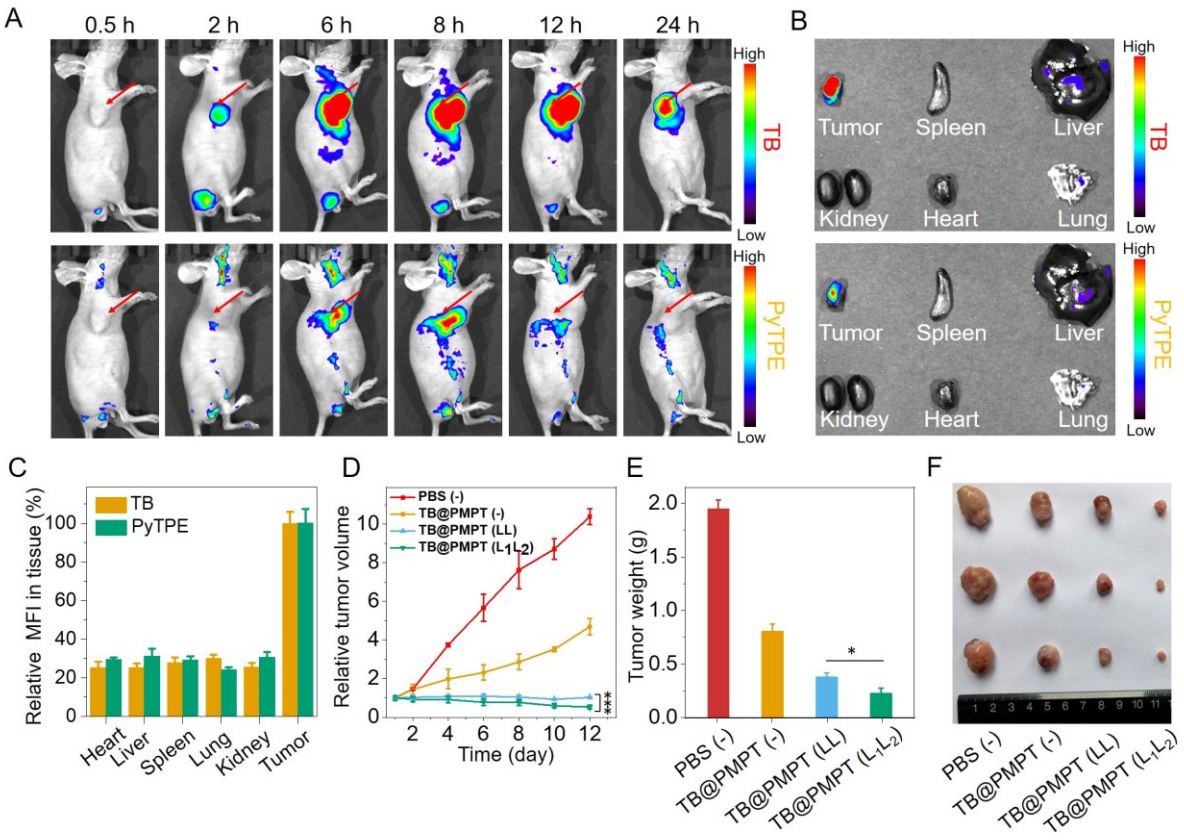

Figure 4. *In vivo* imaging and combinational therapy efficacy. (A) Optical imaging of HeLa tumor-bearing mice after the intravenous injection of TB@PMPT micelles at different time. (B) Fluorescence images and (C) relative mean fluorescence intensity (MFI) of the major organs and tumor of the TB@PMPT micelles treated mice at 24 h post injection (n = 3). (D) Relative tumor volume and (E) tumor weight in the mice after the intravenous of different samples: PBS (-), TB@PMPT (-), TB@PMPT (LL), TB@PMPT (L_1L_2) (LL: samples received 24-min continuous irradiation; L_1L_2: samples received dual-stage light irradiation, 6-min for L_1 and 18-min for L_2, 532 nm, 250 mW cm^{-2}). (F) Representative tumor images of the different groups after 12 days intravenous injection treatment. Data was reported as mean ± SD and analysed through two-sided Student's *t*-test. (*$p < 0.05$)

EXPERIMENTAL SECTION

Materials. 2-Bromoethanol, 2,2′-bipyridine, 3,3′-dithiodipropionic acid, 3-bromopropyne, copper chloride, diethyl methylmalonate, NaH, $LiAlH_4$ and paclitaxel were used as received. Phosphate-buffered saline (PBS), Dulbecco's Modified Eagle's Medium (DMEM), bovine serum albumin (BSA), trypsin and penicillin-streptomycin were purchased from GIBCO Invitrogen Corporation.

Cell culture. HeLa cell line was purchased from the China Center for Type Culture Collection (Wuhan, China). The cells were cultured in DMEM supplemented with 10% fetal bovine serum (FBS) with 1% penicillin and 1% streptomycin at 37 ℃ in a 5% CO_2 atmosphere and 100% humidity.

Animals. BALB/c mice (4-6 weeks old, average body weight 16-18 g) were purchased from HFK Bioscience Co. (Beijing, China). HeLa cells (1×10^6 per mouse) were injected subcutaneously into the right flank of BALB/c mice to generate the tumor mode. All animals received care in compliance with the guidelines set by the Animal Care Committee at Tongji Medical College. Tumor volumes were measured every other day using a caliper and calculated using the following formula: volume = ((tumor length) × (tumor width)^2)/2.

Characterizations. ^{1}H Nuclear magnetic resonance (^{1}H NMR) spectrum were measured by Bruker AM 400 apparatus. The solvent included $CDCl_3$ and DMSO-d_6, and the internal reference was tetra-methylsilane (TMS). The copolymer composition of PEG-*b*-PMPMC (PM) and PEG-*b*-PMPMC-*g*-PTX-*g*-PyTPE (PMPT) was calculated from the ^{1}H NMR spectrum. The average size of micelles was measured by

dynamic light scattering (DLS, Nano-ZS ZEN3690 Malvern Instruments). The morphology of micelles was observed by transmission electron microscopy (TEM, JEM-2100 microscope). High performance liquid chromatography (Agilent 1260) and liquid chromatograph mass spectrometry (LCMS, Thermo) were used to determine the drug release.

Synthesis of PEG-*b*-PMPMC-*g*-PTX-*g*-PyTPE (PMPT). PTX-SS-N_3, PyTPE, PM and 2,2′-bipyridine were dissolved in dry DMF in a Schlenk flask, CuBr was added after two freeze-pump-thaw cycles. The reaction was carried out for two days at 40 ° C in an Ar atmosphere. The crude product solution was purified by Al_2O_3 chromatography and then precipitated three times in ether. Then, the product was purified by dialysis against DMSO for two days.

Determination of critical micelles concentration (CMC) of PMPT. PMPT solutions with or without pretreated with 2, 10 and 50 mM DTT for 1 h were added into sample bottles. The fluorescence emission intensity of PyTPE was analyzed as a function of the PMPT concentration (Ex = 400 nm, Em = 583 nm). When extrapolating the intensity of PMPT concentration region, the CMC values are determined as crossing points.

Preparation of PMPT and TB@PMPT micelles. TB@PMPT micelles were prepared by dialysis in the dark. PMPT (10 mg) and TB (1.2 mg) were dissolved in THF (2 mL), ultrapure water (9 mL) was then slowly added to that solution. The solution of PMPT and TB was transferred to the dialysis tube and dialyzed against ultrapure water for two days. The preparation method of PMPT micelles is similar to that of TB@PMPT micelles.

The drug loading content of PTX, PyTPE and TB. The drug loading contents (DLC) of PTX, TB and PyTPE was determined by HPLC. Briefly, lyophilized nanoparticles (2 mg) were dissolved in THF, the DLC of PTX, PyTPE and TB was determined by HPLC.

***In vitro* PTX release.** PMPT and TB@PMPT micelles were continuously vibrated at 37°C in the dark with or without 10 mM GSH. Samples from the solution (1 mL) were taken out at different time points for HPLC analysis and replaced with 1 mL of fresh medium. The released PTX and PTX-SH from the micelles was evaluated by HPLC (CH_3CN/H_2O = 60/40, v/v; 1.0 mL min^{-1}).

Measurement of ROS generation in solution. ABDA was employed to measure ROS generation of micelles upon light irradiation. ABDA solution (15 μL, 4.5 mg mL^{-1} in DMSO) was mixed to TB@PMP (30 μg mL^{-1}), PMPT (27 μg mL^{-1}) and TB@PMPT (30 μg mL^{-1}) micelles. Then, the mixed solution was irradiated under the with light (white light, 70 mW cm^{-2}). The absorption of ABDA at 400 nm was recorded at various irradiation times to obtain the decay rate of photosensitizing process.

Measurement of ROS generation in living cells. PMPT (94 μg mL^{-1}) and TB@PMPT (105 μg mL^{-1}) micelles were pretreated with or without 10 mM DTT for 1 h in the dark at 37 °C. Subsequently, then the micelles incubated with HeLa cells for 4 h. DCFH-DA (final concentration 1×10^{-5} M) was added into the cells. After 20-min incubation, light irradiation (white light, 70 mW cm^{-2}, 6 min) was performed subsequently. The fluorescence images of cells were obtained using CLMS (Zeiss LSM 880). DCFH (green fluorescence, Ex: 488 nm, Em: 505-540 nm).

Detection of microtubules in cells. PM and PMPT micelles were incubated with the cells in dark for 8 and 16 h, respectively, the concentration of micelles were 54 μg mL^{-1}. Then, the cells were fixed with 4% paraformaldehyde, permeabilized with 0.1% Triton X-100 in PBS and stained with anti-α-tubulin-FITC in the dark for 1 h at 37 °C. Anti-α-tubulin-FITC (green fluorescence, Ex: 488 nm, Em: 505-540 nm)

The reductive environment response of TB@PMPT micelles in tumor cells. PMPT (188 μg mL^{-1}) and TB@PMPT (210 μg mL^{-1}) were incubated with the cells for 2h in dark, respectively. Then the cells were washed three time and further incubated for the predetermined time intervals. The image of cells were observed by CLSM (Zeiss LSM 880). PyTPE (yellow fluorescence, Ex: 405 nm, Em: 500-560 nm), TB (red fluorescence, Ex: 543 nm, Em: 620-720 nm).

The release profiles of PTX from PMPT micelles in aqueous. The release profiles of PTX from PMPT micelles were studied at 37 °C in PBS (10 mM, pH 7.4) containing 0.1% (w/v) Tween 80 with or without 10mM GSH by dialysis method. 4 mL of release medium was replaced with an equal volume of fresh media at predetermined time intervals, the release medium was freeze-dried to obtain the released PTX. The concentration of paclitaxel was determined by UV-vis spectrophotometer.

PTX release in cells. The PTX release in cells was studied as follows. After HeLa cells were seeded in 6-well plates and cultured for 24 h at 37 ℃, then TB@PMPT micelles (210 μg mL^{-1}) were added. After incubation for 2 h at 37 ℃ in dark, the cells were replaced with PBS. At predetermined time intervals, cells were digested by trypsin, harvested by centrifugation, and resuspended in PBS. Cell suspension was freeze-thaw

for three times under -20 ℃, broken using cell disruptor. The broken cell suspension was centrifuged, and the supernatant was analyzed by HPLC (CH_3CN/H_2O =60/40, v/v; 1 mL min^{-1}). The cells treated with culture medium were used as a blank control.

Cellular uptake analysis. HeLa cells were seeded in petri dishes and treated with TB@PM (94 μg mL^{-1}) and TB@PMPT (105 μg mL^{-1}) micelles for 1 h in dark. Then light irradiation (white light, 70 mW cm^{-2}) was performed and incubation with cells continued for 3 h. LysoTracker Green was added and incubated with cells for 0.5 h to identify the intracellular drug location by CLSM. Also, the fluorescence signal of TB and Honest 33258 in HeLa cells recorded after 4 h of incubation with TB@PM and TB@PMPT micelles, respectively. Then, the culture medium was removed and the cells were washed three times with PBS. Then the cells were fixed with 4% paraformaldehyde and the nuclei were stained with Hoechst 33258. Blue fluorescence (nucleus dyed with Hoechst 33258, Ex: 405 nm, Em: 425-475 nm); red fluorescence (TB, Ex: 543 nm, Em: 620-720 nm).

CCK-8 assay. 96-well plate was used to culture HeLa cells of 1×10^4 of cell suspension incubated for 24 h. Subsequently, micelles (200 μL) were added, and that cell were incubated for 1 h before the first light irradiation (L_1, 6 min, white light, 70 mW cm^{-2}). After incubation with cells for 3 h, the cells were exposed to the second light irradiation (L_2, 18 min, white light, 70 mW cm^{-2}). The micelles were removed and incubated for another 44 h before analysis. Cell viability was assessed by the CCK-8 assay.

Hemolysis test. The release of hemoglobin from mice blood cells was used to evaluate the hemolytic activities of PMPT and TB@PMPT micelles, 2 mL red blood cells (4%)

suspension mixed with 0.2 mL phosphate buffer saline (PBS) and 0.2 mL H_2O were served as negative control (no hemolysis) and positive control (100% hemolysis), respectively. PMPT and TB@PMPT micelles of PBS solution (0.2 mL) with different concentration were added into the mixture of 0.2 mL red blood cells suspension. After kept at 37 °C for 6 h in dark, all the samples were centrifuged. The hemolysis ratio of red blood cells was calculated using the following formula: hemolysis (%) = (A_{sample} - $A_{negative}$)/($A_{positive}$ - $A_{negative}$) × 100%, where A_{sample}, $A_{negative}$, and $A_{positive}$ refer to the absorption of material sample solution, negative control, and positive control at 570 nm, respectively.

Biodistribution *in vivo*. After the tumor volume reached to ~100 mm^3, the TB@PMPT micelles were intravenously injected into the tumor-bearing BALB/c nude mice at the concentration of 2.0 mg mL^{-1} in PBS through tail vein. Mice were anesthetized at predetermined time points and imaged by small animal imaging system in Institute of Virology (PerkinElmer). For tissue distribution studies, the mice were sacrificed at 24 hours after injection. Heart, liver, spleen, lungs, kidneys and tumors were exfoliated and imaged.

Antitumor activity *in vivo*. The mice were randomly divided into four groups, and intravenously injected with PBS (-), TB@PMPT (without light irradiation, 2.0 mg mL^{-1}), TB@PMPT (LL, 24 min light irradiation for PDT, 2.0 mg mL^{-1}), and TB@PMPT (L_1L_2, 6 min light irradiation to enhance endocytosis and an 18 min light irradiation for PDT, 2.0 mg mL^{-1}) respectively on the first, fourth, seventh, and tenth days. The dose of TB@PMPT was 12.5 mg kg^{-1} per mouse. The 6 min light irradiation

was performed after injection for 6 h (L_1, 532 nm, 250 mW cm^{-2}), the 18 min light irradiation (L_1) and the 24 min light irradiation (LL)were all performed after injection for 8 h (532 nm, 250 mW cm^{-2}). Relative tumor volume and body weight was defined as V/V_0 and W/W_0, respectively (V_0 and W_0 was the tumor volume and body weight on the first day before treatment). After the mice were sacrificed, muscle, heart, liver, spleen, lung, kidney and tumor tissue were collected and stained with H&E staining.

Data availability. Data supporting the findings of this study are available within this article and its Supplementary Information file, and from the corresponding author on reasonable request.

ASSOCIATED CONTENT

Supporting Information

The Supporting Information is available free of charge at http://pubs.acs.org.

Synthetic routes to PMPT; ^{1}H NMR, ESI-MS spectra of compounds; UV-vis absorption spectrum of TB@PMPT micelles; MS and HPLC analyses of PMPT micelles; DLS results of PMPT and TB@PMPT micelles; CLSM images of TB@PMPT micelles-treated HeLa cells; *in vitro* cytotoxicities of micelles; tumor growth.

AUTHOR INFORMATION

Corresponding Author

*E-mail：louxiaoding@cug.edu.cn (X. Lou)

*E-mail：xiafan@cug.edu.cn (F. Xia)

*E-mail：tangbenz@ust.hk (B. Z. Tang)

Author Contributions

The manuscript was written through contributions of all authors. All authors have given approval to the final version of the manuscript.

Statement

The manuscript have been previously submitted to a pre-print of ChemRxiv. Yi, X.; Lou, X.; Zhao, Z.; Xia, F.; Tang, B. Z. Self-Guiding Polymeric Prodrug Micelles with Two AIE Photosensitizers for Enhanced Chemo-Photodynamic Therapy. 2020, ChemRxiv. Preprint. https://doi.org/10.26434/chemrxiv.13160750.v1.

ACKNOWLEDGMENT

This work is supported by the National Key R&D Program of China (2020YFA0211200), the National Natural Science Foundation of China (21788102, 21974128, 21874121), the Natural Science Foundation of Hubei Province (2019CFA043), the Talents' Start-up Fund of Gannan Medical University (QD201903), the Open Project of Key Laboratory of Prevention and Treatment of Cardiovascular and Cerebrovascular Diseases, Ministry of Education (XN201911). Dr. Yuqiu Ke in Jiangxi University of Science and Technology and Dr. Ying Kuang in Gannan Medical University are thanked for their helps in manuscript revisions and cell experiments, respectively.

REFERENCES

(1) Wang, D.; Wu, H.; Yang, G.; Qian, C.; Gu, L.; Wang, H.; Zhou, W.; Liu, J.; Wu, Y.; Zhang, X.;.Guo, Z.; Chen, H.; Jana, D.; Zhao, Y. Metal-Organic Framework

Derived Multicomponent Nanoagent as a Reactive Oxygen Species Amplifier for Enhanced Photodynamic Therapy. *ACS Nano* **2020**, *14* (10), 13500-13511.

(2) Xu, M.; Wang, X.; Wang, Q.; Hu, Q.; Huang, K.; Lou, X.; Xia, F. Analyte-Responsive Fluorescent Probes with AIE Characteristic Based on the Change of Covalent Bond. *Sci. China-Mater*. **2019**, *62* (9), 1236-1250.

(3) Luo, J. D.; Xie, Z. L.; Lam, J. W. Y.; Cheng, L.; Chen, H. Y.; Qiu, C. F.; Kwok, H. S.; Zhan, X. W.; Liu, Y. Q.; Zhu, D. B.; Tang, B. Z. Aggregation-Induced Emission of 1-methyl-1,2,3,4,5-pentaphenylsilole. *Chem. Commun*. **2001**, (18), 1740-1741.

(4) Dai, J.; Li, Y.; Long, Z.; Jiang, R.; Zhuang, Z.; Wang, Z.; Zhao, Z.; Lou, X.; Xia, F.; Tang, B. Z. Efficient Near-Infrared Photosensitizer with Aggregation-Induced Emission for Imaging-Guided Photodynamic Therapy in Multiple Xenograft Tumor Models. *ACS Nano* **2020**, *14* (1), 854-866.

(5) Cheng, Y.; Dai, J.; Sun, C.; Liu, R.; Zhai, T.; Lou, X.; Xia, F. An Intracellular H_2O_2-Responsive AIEgen for the Peroxidase-Mediated Selective Imaging and Inhibition of Inflammatory Cells. *Angew. Chem. Int. Ed*. **2018**, *57* (12), 3123-3127.

(6) Gu, X.; Zhang, X.; Ma, H.; Jia, S.; Zhang, P.; Zhao, Y.; Liu, Q.; Wang, J.; Zheng, X.; Lam, J. W. Y.; Ding, D.; Tang, B. Z. Corannulene-Incorporated AIE Nanodots with Highly Suppressed Nonradiative Decay for Boosted Cancer Phototheranostics *in Vivo*. *Adv. Funct. Mater.* **2018**, *30* (26), 1801065.

(7) Zhen, S.; Wang, S.; Li, S.; Luo, W.; Gao, M.; Ng, L. G.; Goh, C. C.; Qin, A.; Zhao, Z.; Liu, B.; Tang, B. Z. Efficient Red/Near-Infrared Fluorophores Based on Benzo[1,2-b:4,5-b']dithiophene 1,1,5,5-tetraoxide for Targeted Photodynamic Therapy and *in Vivo* Two-Photon Fluorescence Bioimaging. *Adv. Funct. Mater.* **2018**, *28* (13), 1706945.

(8) Cai, X.; Mao, D.; Wang, C.; Kong, D.; Cheng, X.; Liu, B. Multifunctional Liposome: A Bright AIEgen-Lipid Conjugate with Strong Photosensitization. *Angew. Chem. Int. Ed*. **2018**, *57* (50), 16396-16400.

(9) Cheng, Y.; Sun, C.; Liu, R.; Yang, J.; Dai, J.; Zhai, T.; Lou, X.; Xia, F. A Multifunctional Peptide-Conjugated AIEgen for Efficient and Sequential Targeted Gene Delivery into the Nucleus. *Angew. Chem. Int. Ed.* **2019**, *58* (15), 5049-5053.

(10) Yuan, Q.; Cheng, Y.; Lou, X.; Xia, F. Rational Fabrication and Biomedical Application of Biomolecule-Conjugated AIEgens through Click Reaction. *Chin. J. Chem.* **2019**, *37* (10), 1072-1082.

(11) Wang, Q.; Wang, X.; Xu, M.; Lou, X.; Xia, F. One-Dimensional and Two-Dimensional Nanomaterials for the Detection of Multiple Biomolecules. *Chin. Chem. Lett.* **2019**, *30* (9), 1557-1564.

(12) Ou, X.; Lou, X.; Xia, F. A Highly Sensitive DNA-AIEgen-Based "Turn-On" Fluorescence Chemosensor for Amplification Analysis of Hg^{2+} Ions in Real Samples and Living Cells. *Sci. China-Chem.* **2017**, *60* (5), 663-669.

(13) Xia, F.; Wu, J.; Wu, X.; Hu, Q. Y.; Dai, J.; Lou, X. D. Modular Design of Peptide- or DNA-Modified AlEgen Probes for Biosensing Applications. *Accounts Chem. Res.* **2019**, *52* (11), 3064-3074.

(14) Meng, Q. S.; Meng, J.; Ran, W.; Wang, J. Y.; Zhai, Y. H.; Zhang, P. C.; Li, Y. P. Light-Activated Core-Shell Nanoparticles for Spatiotemporally Specific Treatment of Metastatic Triple-Negative Breast Cancer. *ACS Nano* **2018**, *12* (3), 2789-2802.

(15) Pei, Q.; Hu, X. L.; Zheng, X. H.; Liu, S.; Li, Y. W.; Jing, X. B.; Xie, Z. G. Light-Activatable Red Blood Cell Membrane-Camouflaged Dimeric Prodrug Nanoparticles for Synergistic Photodynamic/Chemotherapy. *ACS Nano* **2018**, *12* (2), 1630-1641.

(16) Guan, Q.; Zhou, L. L.; Li, Y. A.; Li, W. Y.; Wang, S. M.; Song, C.; Dong, Y. B. Nanoscale Covalent Organic Framework for Combinatorial Antitumor Photodynamic and Photothermal Therapy. *ACS Nano* **2019**, *13* (11), 13304-13316.

(17) Li, L. P.; Li, J. Y.; Shi, Y. X.; Du, P.; Zhang, Z. Z.; Liu, T.; Zhang, R. P.; Liu, Z. B. On-Demand Biodegradable Boron Nitride Nanoparticles for Treating Triple Negative Breast Cancer with Boron Neutron Capture Therapy. *ACS Nano* **2019**, *13* (12), 13843-13852.

(18) Cherkasov, V. R.; Mochalova, E. N.; Babenyshev, A. V.; Vasilyeva, A. V.; Nikitin, P. I.; Nikitin, M. P. Nanoparticle Beacons: Supersensitive Smart Materials with On/Off-Switchable Affinity to Biomedical Targets. *ACS Nano* **2020**, *14* (2), 1792-1803.

(19) Hunt, N. J.; Lockwood, G. P.; Le Couteur, F. H.; McCourt, P. A. G.; Singla, N.; Kang, S. W. S.; Burgess, A.; Kuncic, Z.; Le Couteur, D. G.; Cogger, V. C. Rapid

Intestinal Uptake and Targeted Delivery to the Liver Endothelium Using Orally Administered Silver Sulfide Quantum Dots. *ACS Nano* **2020**, *14* (2), 1492-1507.

(20) Hu, X. L.; Hu, J. M.; Tian, J.; Ge, Z. S.; Zhang, G. Y.; Luo, K. F.; Liu, S. Y. Polyprodrug Amphiphiles: Hierarchical Assemblies for Shape-Regulated Cellular Internalization, Trafficking, and Drug Delivery. *J. Am. Chem. Soc.* **2013**, *135* (46), 17617-17629.

(21) Li, D.; Tang, Z. M.; Gao, Y. Q.; Sun, H. L.; Zhou, S. B. A Bio-Inspired Rod-Shaped Nanoplatform for Strongly Infecting Tumor Cells and Enhancing the Delivery Efficiency of Anticancer Drugs. *Adv. Funct. Mater.* **2016**, *26* (1), 66-79.

(22) Cheng, D.-B.; Zhang, X.-H.; Gao, Y.-J.; Ji, L.; Hou, D.; Wang, Z.; Xu, W.; Qiao, Z.-Y.; Wang, H. Endogenous Reactive Oxygen Species-Triggered Morphology Transformation for Enhanced Cooperative Interaction with Mitochondria. *J. Am. Chem. Soc.* **2019**, *141* (18), 7235-7239.

(23) Cai, H.; Dai, X. H.; Wang, X. M.; Tan, P.; Gu, L.; Luo, Q.; Zheng, X. L.; Li, Z. Q.; Zhu, H. Y.; Zhang, H.; Gu, Z. W.; Gong, Q. Y.; Luo, K. A Nanostrategy for Efficient Imaging-Guided Antitumor Therapy through a Stimuli-Responsive Branched Polymeric Prodrug. *Adv. Sci*. **2020**, *7* (6), 1903243.

(24) Li, H. J.; Du, J. Z.; Du, X. J.; Xu, C. F.; Sun, C. Y.; Wang, H. X.; Cao, Z. T.; Yang, X. Z.; Zhu, Y. H.; Nie, S. M.; Wang, J. Stimuli-Responsive Clustered Nanoparticles for Improved Tumor Penetration and Therapeutic Efficacy. *Proc. Natl. Acad. Sci. U. S. A.* **2016**, *113* (15), 4164-4169.

(25) Ghosh, S.; Carter, K. A.; Lovell, J. F. Liposomal Formulations of Photosensitizers. *Biomaterials* **2019**, *218*, 119341.

(26) Han, K.; Wang, S.-B.; Lei, Q.; Zhu, J.-Y.; Zhang, X.-Z. Ratiometric Biosensor for Aggregation-Induced Emission-Guided Precise Photodynamic Therapy. *ACS Nano* **2015**, *9* (10), 10268-10277.

(27) Wang, Y.; Wei, G.; Zhang, X.; Xu, F.; Xiong, X.; Zhou, S. A Step-by-Step Multiple Stimuli-Responsive Nanoplatform for Enhancing Combined Chemo-Photodynamic Therapy. *Adv. Funct. Mater*. **2017**, *29* (12), 605357.

(28) Cheng, H.; Fan, J.-H.; Zhao, L.-P.; Fan, G.-L.; Zheng, R.-R.; Qiu, X.-Z.; Yu, X.-Y.; Li, S.-Y.; Zhang, X.-Z. Chimeric Peptide Engineered Exosomes for Dual-Stage Light Guided Plasma Membrane and Nucleus Targeted Photodynamic Therapy. *Biomaterials* **2019**, *211*, 14-24.

(29) Han, K.; Lei, Q.; Wang, S.-B.; Hu, J.-J.; Qiu, W.-X.; Zhu, J.-Y.; Yin, W.-N.; Luo, X.; Zhang, X.-Z. Dual-Stage-Light-Guided Tumor Inhibition by Mitochondria-Targeted Photodynamic Therapy. *Adv. Funct. Mater.* **2015**, *25* (20), 2961-2971.

(30) Prasmickaite, L.; Hogset, A.; Tjelle, T. E.; Olsen, V. M.; Berg, K. Role of Endosomes in Gene Transfection Mediated by Photochemical Internalisation (PCI). *J. Gene. Med.* **2000**, *2* (6), 477-488.

(31) Cheng, H.; Fan, G. L.; Fan, J. H.; Zhao, L. P.; Zheng, R. R.; Yu, X. Y.; Li, S. Y. Ratiometric Theranostic Nanoprobe for pH Imaging-Guided Photodynamic Therapy. *Nanoscale* **2019**, *11* (18), 9008-9014.

(32) Li, S.-Y.; Cheng, H.; Xie, B.-R.; Qiu, W.-X.; Song, L.-L.; Zhuo, R.-X.; Zhang, X.-Z. A Ratiometric Theranostic Probe for Tumor Targeting Therapy and Self-Therapeutic Monitoring. *Biomaterials* **2016**, *104*, 297-309.

(33) Yi, X.; Zhao, D.; Zhang, Q.; Xu, J.; Yuan, G.; Zhuo, R.; Li, F. A Co-Delivery System Based on a Reduction-Sensitive Polymeric Prodrug Capable of Loading Hydrophilic and Hydrophobic Drugs for Combination Chemotherapy. *Polym. Chem.* **2016**, *7* (38), 5966-5977.

(34) Cheng, Y.; Huang, F.; Min, X.; Gao, P.; Zhang, T.; Li, X.; Liu, B.; Hong, Y.; Lou, X.; Xia, F. Protease-Responsive Prodrug with Aggregation-Induced Emission Probe for Controlled Drug Delivery and Drug Release Tracking in Living Cells. *Anal. Chem.* **2016**, *88* (17), 8913-8919.

(35) Chen, C.; Song, Z.; Zheng, X.; He, Z.; Liu, B.; Huang, X.; Kong, D.; Ding, D.; Tang, B. Z. AIEgen-Based Theranostic System: Targeted Imaging of Cancer Cells and Adjuvant Amplification of Antitumor Efficacy of Paclitaxel. *Chem. Sci.* **2017**, *8*, 2191-2198.

(36) Yi, X.; Dai, J.; Han, Y.; Xu, M.; Zhang, X.; Zhen, S.; Zhao, Z.; Lou, X.; Xia, F. A High Therapeutic Efficacy of Polymeric Prodrug Nano-Assembly for a Combination of Photodynamic Therapy and Chemotherapy. *Commun. Biol.* **2018**, *1* (1), 202.

(37) French, A. P.; Mills, S.; Swarup, R.; Bennett, M. J.; Pridmore, T. P. Colocalization of Fluorescent Markers in Confocal Microscope Images of Plant Cells. *Nat. Protoc.* **2008**, *3* (4), 619-628.

(38) Mukaka, M. M. Statistics Corner: A Guide to Appropriate Use of Correlation Coefficient in Medical Research. *Malawi Med. J.* **2012**, *24* (3), 69-71.

(39) Ma, S.; Song, W.; Xu, Y.; Si, X.; Zhang, D.; Lv, S.; Yang, C.; Ma, L.; Tang, Z.; Chen, X. Neutralizing Tumor-Promoting Inflammation with Polypeptide-Dexamethasone Conjugate for Microenvironment Modulation and Colorectal Cancer Therapy. *Biomaterials* **2020**, *232*, 119676-119676.

(40) Liu, L.-H.; Qiu, W.-X.; Zhang, Y.-H.; Li, B.; Zhang, C.; Gao, F.; Zhang, L.; Zhang, X.-Z. A Charge Reversible Self-Delivery Chimeric Peptide with Cell Membrane-Targeting Properties for Enhanced Photodynamic Therapy. *Adv. Funct. Mater.* **2017**, *27* (25), 1700220.

(41) Yin, S.; Huai, J.; Chen, X.; Yang, Y.; Zhang, X.; Gan, Y.; Wang, G.; Gu, X.; Li, J. Intracellular Delivery and Antitumor Effects of a Redox-Responsive Polymeric Paclitaxel Conjugate Based on Hyaluronic Acid. *Acta Biomater.* **2015**, *26*, 274-285.

(42) Hu, Y. W.; Du, Y. Z.; Liu, N.; Liu, X.; Meng, T. T.; Cheng, B. L.; He, J. B.; You, J.; Yuan, H.; Hu, F. Q. Selective Redox-Responsive Drug Release in Tumor Cells Mediated by Chitosan Based Glycolipid-Like Nanocarrier. *J. Control. Release* **2015**, *206*, 91-100.

(43) Zhou, L.; Lv, F.; Liu, L.; Shen, G.; Yan, X.; Bazan, G. C.; Wang, S. Cross-Linking of Thiolated Paclitaxel-Oligo(*p*-phenylene vinylene) Conjugates Aggregates inside Tumor Cells Leads to "Chemical Locks" That Increase Drug Efficacy. *Adv. Funct. Mater.* ***2018***, *30* (10), 1704888.

(44) Perry, J. L.; Reuter, K. G.; Luft, J. C.; Pecot, C. V.; Zamboni, W.; DeSimone, J. M. Mediating Passive Tumor Accumulation through Particle Size, Tumor Type, and Location. *Nano Lett*. **2017**, *17* (5), 2879-2886.

SYNOPSIS (Word Style “SN_Synopsis_TOC”).